Chaos, Solitons and Fractals 165 (2022) 112774

Contents lists available at ScienceDirect

Chaos, Solitons and Fractals

journal homepage: www.elsevier.com/locate/chaos

Non-Hermitian control of optical turbulence in systems with fractional dispersion

Salim B. Ivars [a,*], Muriel Botey [a], Ramon Herrero [a], Kestutis Staliunas [a,b,c]

[a] Departament de Física, Universitat Politècnica de Catalunya (UPC), Rambla Sant Nebridi 22, 08222, Terrassa, Barcelona, Catalonia, Spain
[b] Institució Catalana de Recerca i Estudis Avançats (ICREA), Passeig Lluís Companys 23, E-08010, Barcelona, Spain
[c] Vilnius University, Faculty of Physics, Laser Research Center, Sauletekio Ave. 10, Vilnius, Lithuania

A B S T R A C T

We show an efficient mechanism to control optical turbulence in systems with different dispersion laws, including parabolic, sub-diffractive, hyper-diffractive or general fractional dispersion. The method is based on the modification of the energy cascade through spatial scales leading to turbulence: a non-Hermitian spatio-temporal periodic potential allows unidirectional coupling between modes in the excitation process. We prove a significant increase and reduction of the energy flow in turbulent states, by either condensing the excitation towards small wave-numbers or affecting the energy transfer towards large wave-number. The study is based on the complex Fractional Ginzburg–Landau equation, a universal model for pattern formation and turbulence in a wide range of systems. The enhancement or reduction of turbulence is indeed dependent on the imposed direction of the energy flow, controlled by the phase shift between the real and imaginary parts of the temporal oscillation of the non-Hermitian potential.

1. Introduction

Throughout history, the turbulence has attracted the interest of many scientist, yet remaining a long-standing problem. Only in the last century, the efforts of Landau [1], Kolmogorov [2], Richardson [3], Arnold [4], Lorentz [5] and others, have led to the quantitative theory of turbulence. Such research was crowned by the so called $-5/3$ Kolmogorov law which states that, in the full developed hydrodynamical turbulence, energy is distributed among spatial scales as: $E(k) \sim k^{-5/3}$ [2,6], see Fig. 1. Specifically, the system is excited at large spatial scales, (being $k_{excit} \sim 1/d_{excit}$ small), yet energy dissipates at a smaller scale, the viscosity scale (where $k_{visc} \sim 1/d_{visc}$ is large). In the inertial range, between these excitation and dissipation scales, the energy of excitation migrates forming this particular $-5/3$ power law.

Whereas this energy cascading power law is strictly valid in a 3-dimensional (3D) space holding isotropic, homogeneous, and well-developed turbulence, other configurations, for instance the turbulence in 2D, may also follow an analogous scheme. Qualitatively, the idea of the excitation cascade through spatial scales (or equivalently, through spatial wavenumbers) is applicable to a wide range of physical systems. A major class of turbulent systems follow the same general picture: energy is injected on a large spatial scale in continuous systems, migrates though spatial scales to be dissipated on a small scale. Therefore, turbulence "bridges" energy between these two spatial scales.

It can be expected that this general principle holds likewise in optical turbulence, which is predominantly a 2D phenomenon restricted within the transverse plane of laser resonators, where electromagnetic transverse modes induce pattern formation and filamentation [7–11]. Yet 1D patterns are relevant for broad aperture planar cavities as well as 3D patterns are applicable for multilongitudinal and multitransversal mode lasers. Differently from the hydrodynamical turbulence, optical transverse modes are excited in a wider range of spatial scales, and dissipated at smaller scales, see the schematic representation on Fig. 1 (c). In lasers, the gain is coherent, which, mathematically speaking, is a multiplicative effect, as photons multiply in each transverse mode. Besides, losses occur for light propagating at large angles with respect to the optical axis (limited either by the geometry or other intrinsic filtering mechanisms), *i.e.* for small scales in the transverse space possibly leading to excitation cascades, see Fig. 1 (d).

Different attempts of controlling the turbulence have been proposed, for instance by means of delayed global feedback [12–14], local injections [15,16] or localised inhomogeneities [14,17]. Recently, a new approach based on a dynamical non-Hermitian potentials was proposed [18]. The potentials periodic in space and time indeed showed the ability to control the cascades of optical turbulence. That study [18] is based on the complex Ginzburg–Landau Equation (CGLE), a universal model for pattern formation and turbulence in a wide range of systems including nonlinear optical resonators.

The present article presents a generalisation of the non-Hermitian turbulence control. We explore the robustness of the turbulence control mechanism to systems with fractional dispersion. After an overview of the results of non-Hermitian turbulence control for a usual parabolic

* Corresponding author.
E-mail address: salim.benadouda@upc.edu (S.B. Ivars).

https://doi.org/10.1016/j.chaos.2022.112774
Received 19 July 2022; Received in revised form 18 September 2022; Accepted 1 October 2022
Available online 27 October 2022

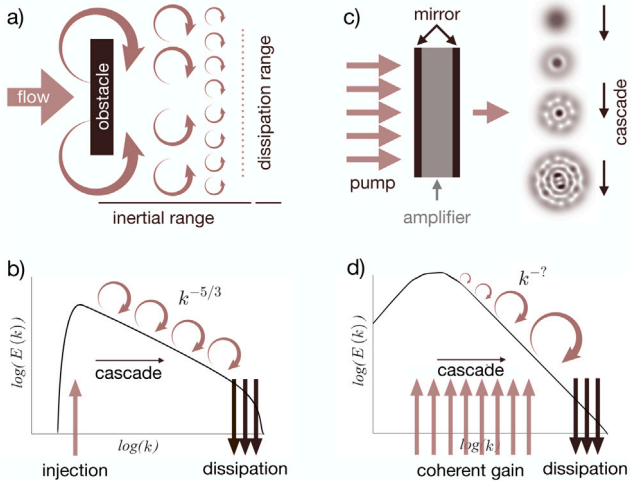

Fig. 1. (a) Excitation cascade of a hydrodynamical turbulent system; and (b) excitation distributions through the spatial scales for fully developed hydro-dynamical turbulence, resulting in the celebrated Kolmogorov -5/3 power law in the inertial range. (c) Scheme of the optical turbulence in broad aperture lasers; and (d) hypothetical excitation cascade in optical turbulence, even in the absence of inertial range.

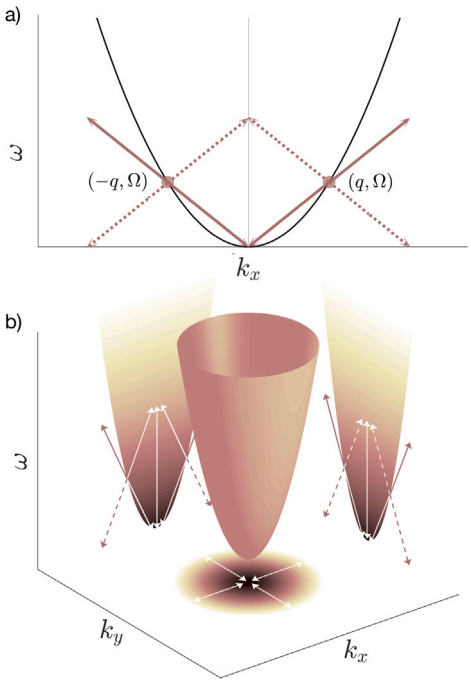

Fig. 2. Proposed mechanism on a parabolic dispersion. (a) 1D parabolic dispersion curve $\omega = k_x^2$, and corresponding (b) dispersion paraboloid in 2D $\omega = k_x^2 + k_y^2$. Arrows, in both figures, indicate all possible symmetric mode couplings for an Hermitian modulation in the form: $V(\mathbf{r}) = \cos(qx)\cos(\Omega t)$, dashed arrows correspond to non-functional couplings while solid arrows correspond to functional couplings.

dispersion, we extend the study to conical dispersion, where the conical dispersion may be regarded as hyper-diffraction. Next we also provide analogous results for a non-integer diffraction order, and even a sub-diffractive case with fourth order diffraction is considered. We finally prove the proposal in 2D, for parabolic and conical dispersion, as an example.

2. Model and turbulence control proposal

The CGLE is a universal model for pattern formation and turbulence in a wide range of systems covering from nonlinear optical resonators to second-order phase transitions, from superconductivity, superfluidity, and Bose–Einstein condensation to liquid crystals and strings in field theory [19]. Expressed in one of its several possible conventions, it reads:

$$\frac{\partial A}{\partial t} = (1 - i\alpha)\left(1 - |A|^2\right)A + (i + d)\,\nabla^2 A + V(\mathbf{r}, t)A \tag{1}$$

where, the order parameter $A(\mathbf{r}, t)$ is a complex function of time t and space $\mathbf{r}$ (we analyse 1D and 2D systems), α is the self-focusing coefficient, d the diffusion coefficient and $V(\mathbf{r}, t)$ is a complex valued spatio-temporal potential. The gain and dispersion coefficients are normalised to unity, without loss of generality.

Analysing the energy balance in Eq. (1), we note that the gain term is multiplicative, *i.e.* scale invariant. In turn, losses are due to the diffusion, therefore occurring on a small scale. Important term of the CGLE influencing the excitation migration processes is the non-linearity. The saturating part of the Kerr non-linearity basically redistributes the excitation through the space scales (represents a double convolution of modes), and also on overall causes the migration of excitations depending on the dimensionality of the system.

Whilst numerous studies cover laser turbulence [20–23], the energy cascading in CGLE turbulence, or the energy cascading in optical turbulence, has hardly been considered systematically.

All spatially extended dynamical systems hold a particular dispersion law. The dispersion is a dependence of the frequency (energy) on the wave-number (momentum). Concerning spatial laser patterns this dispersion represents the dependence of the mode frequency versus its transverse wave-number (the angular deviation from the optical axis, in the case of lasers). In particular for lasers, the spatial dispersion forms a parabola. In general, the dispersion curve is parity-time symmetric in wave-number domain (the k-symmetry), but asymmetric in frequency domain (the ω-asymmetry). The cloud of the points spreading around the dispersion curve may be obtained by the numerical reconstruction of the dispersion in the CGLE simulated in turbulent regime. Different excitation mixing and migration processes (in the lowest order, basically due to nonlinear four wave mixing, equivalent to two-particle collisions) broaden such cloud of points, located around the dispersion curve, being to some extent limited by dissipation/saturation. The broader the cloud of points the stronger is the turbulence. Controlling the broadening of such turbulence cloud is the ultimate goal of turbulence control. Ideally, for full turbulence control, the cloud would condensate onto a point or a coherent set of points.

Introducing a Hermitian background modulation, either being a temporal and or spatial modulation, does not lead to an effectively control of turbulence due to symmetric mode coupling. The symmetry in the mode coupling induced by a 1D harmonic modulation (in space and time), such as: $\cos(qx + \Omega t)$, can be simply understood by expressing the harmonic modulations as a sum of positive and negative exponent: $\cos(qx + \Omega t) = \left[\exp(iqx + i\Omega t) + \exp(-iqx - i\Omega t)\right]/2$. Each exponent, schematically represented by one of the arrows in Fig. 2 (a), brings the excitation (k_x, ω) towards the central area of dispersion diagram, $(0, 0)$, but simultaneously also towards larger spatial scales. Therefore, a Hermitic modulation of the background potential cannot influence the flows of excitation through the spatial scales.

On the contrary, non-Hermitian potentials have shown to hold asymmetric properties [24–26]. A complex-valued modulation of the potential such as: $\cos(-iqx + i\Omega t) + i\sin(-iqx + i\Omega t) = \exp(-iqx + i\Omega t)$, induces a unidirectional flux of energy towards smaller spatial scales (or towards larger scales, depending on the sign of the argument of the remaining exponent). Such unidirectional mode coupling would only correspond to one arrow from the four couplings represented in Fig. 2 (a). In particular, this may be applied to the simple and universal model of the CGLE to influence the energy cascade in turbulence. In fact, just the temporal part of the potential modulation needs to be non-Hermitian, the spatial part may remain real-valued. In other words, the

parity-time symmetry in the temporal domain must be broken, whereas the symmetry in space is maintained. As a result, the enhancement or reduction of turbulence is expected to be dependent on the imposed direction of the energy flow, controlled by the phase shift between the real and imaginary parts of the temporal oscillation of the non-Hermitian potential. In turn, the necessary resonance imposed by the dispersion relation curve, selects the functional couplings [18].

This is the main idea behind the present proposal of non-Hermitian turbulence control [18]. Interesting are the possible generalisations and robustness of the control to different kinds of non-linearity and different perturbing potentials. Beyond this, and more appealing or fundamental is the persistence of the method for different dispersion. The parabolic dispersion, may be regarded as paraxial approximation, valid for small angle propagation with respect to the optical axis, whilst diffraction is generally spherical in optics. Moreover, recently studies face situations with different types of diffraction due to periodic modulations of the refractive index inside of the laser cavity [27,28]. The dispersion relation of a system can be shaped by spatial modulations of the complex refractive index. For instance, the fourth order dispersion can be obtained by refractive index modulations or simultaneous refraction index and gain modulation [29,30]. The index modulation pushes apart the dispersion surfaces one from another, becoming to flat-top or flat-bottom. In contrary, gain modulations pull dispersion surfaces one to another turning them more sharp-top and sharp-bottom.

One interesting situation is the so called sub-diffractive regime, where the quadratic part of the diffraction disappears and the shape of the dispersion surface $S(k)$ corresponds to the next leading term, the fourth order, $S(k) = \left(k_x^2 + k_y^2\right)^2$ and the diffraction operator in direct space of Eq. (1) takes the form $\left(\partial_x^2 + \partial_y^2\right)^2$ [29,30]. Another interesting and relevant modification of diffraction occurs for the refraction index potentials forming Kagome lattices, for instance around the K point of the reciprocal-space in Graphene. The diffraction surface becomes $S(k) = \left(k_x^2 + k_y^2\right)^{(1/2)}$ and the diffraction operator in Eq. (1) becomes $\left(\partial_x^2 + \partial_y^2\right)^{1/2}$ [31].

For simplicity, the control of turbulence for the different dispersion relations is analysed in 1D while in the final part we provide results in 2D for particular configurations, for being the most usual situation in nonlinear optics. We note that it could be analogously extended to 3D.

All these relevant cases of the modified diffraction can be considered as special orders of fractional diffraction. Recently, versions of some of the most universal equations with partial derivatives, including non-integer numbers are attracting interest. This is the case for the fractional Schrödinger and Fractional Ginzburg–Landau equation that have been studied in mathematics [32,33], finding also its applications in physics [34–37]. The Fractional Complex Ginzburg Landau Equation (FCGLE) can be written in the following form:

$$\frac{\partial A}{\partial t} = (1 - i\alpha)\left(1 - |A|^2\right)A + (i + d)\left(\nabla^2\right)^{\frac{\beta}{2}} A + V(\mathbf{r}, t)A, \tag{2}$$

where the fractional derivative is defined as the integral operator by the Fourier Transform:

$$\left(-\nabla^2\right)^{\frac{\beta}{2}} A = \frac{1}{2\pi}\iint d\mathbf{k}d\mathbf{r}'\,|\mathbf{k}|^\beta \exp\left[i\mathbf{k}\left(\mathbf{r} - \mathbf{r}'\right)\right]A\left(\mathbf{r}'\right). \tag{3}$$

Note that for the quadratic fractional order, $\beta = 2$, we recover the classic CGLE with usual, parabolic dispersion, and for $\beta = 1$ corresponds to a conic dispersion.

3. Results

3.1. Parabolic dispersion $\beta = 2$

The proposed mechanism relies on the introduction of a periodic non-Hermitian potential, which as above discussed, we assume in the form:

$$V(\mathbf{r}, t) = V(\mathbf{r})\left[m_1 \cos(\Omega t) + i m_2 \cos\left(\Omega t + \phi_t\right)\right], \tag{4}$$

where $V(\mathbf{r})$ represents the spatial part of the modulation, Ω corresponds to the temporal modulation frequency, m_1 and m_2 are the amplitudes of the real and imaginary part of the temporal modulation and ϕ_t corresponds to their phase shift. For instance, m_1 controls the gain modulation amplitude, while m_2 corresponds to the refractive index modulation amplitude. For simplicity we have assumed $m_1 = m_2 \equiv m$. Initially, we focus on 1D systems with a spatial harmonic modulation in the form $V(\mathbf{r}) = \cos(qx)$. As commented above, the goal of the proposed mechanism is to influence the spectrum of the system. Thus, we characterise the effect on the spatio-temporal spectrum of the system $A\left(k_x, \omega\right)$, which is the 2D Fourier transform of the field $A(x, t)$, by means of two different spectral intensities. First, the averaged in ω intensity of the spectrum:

$$I\left(k_x\right) = \int \left|A\left(k_x, \omega\right)\right|^2 d\omega. \tag{5}$$

Secondly, the averaged in k_x spectral intensity:

$$I(\omega) = \int \left|A\left(k_x, \omega\right)\right|^2 dk_x. \tag{6}$$

As previously reported it the study made in [18], the strength of the turbulence can be characterised by the normalised central intensity of $I\left(k_x\right)$: $\eta = I(0)/\int I\left(k_x\right)dk_x$, which expresses the level of condensation of the energy into the lowest order mode, the homogeneous component. This parameter does not take into account the coherently excited harmonics. The better the stabilisation, the larger is the value of η, since we would have concentrated the energy at low order modes. On the other hand, we can take into account the full excited comb (in $k-$space and $\omega-$space) since the coherently excited harmonics are not introducing disorder into the system. Therefore, we compute the Full Width at Half Maximum (FWHM) of each spectrum $I\left(k_x\right)$ and $I(\omega)$ sorted by intensity value. As an example, for a perfect comb at $k_x = nq$, the $FWHM_{k_x}$ would be much smaller than for a turbulent distribution. Analogously, this also applies for $FWHM_\omega$.

For $\beta = 2$, as expected, the numerically reconstructed spectrum follows the parabolic dispersion $\omega = k_x^2$. More precisely, the spectrum corresponds to a cloud of points in the $\left(k_x, \omega\right)$ distributed around the dispersion of the linear counterpart system. Fig. 3 (a) and (b) depict the turbulent unmodulated field in the real space and its corresponding spectrum, along with the spectral intensities $I\left(k_x\right)$ and $I(\omega)$, in the two projections. The introduction of a Hermitian harmonic modulation, *i.e.* $m_2 = 0$, induces a modulation of the field in the direct space, see Fig. 3 (c), yet the spectral distribution remains almost unaffected, resembling the unmodulated system, see Fig. 3 (d). Differently, the non-Hermitian modulation totally changes the spectral distribution, concentrating it towards lower order modes for an inward coupling, situation depicted in (e) and (f). The field in the direct space clearly follows the modulation and the spectrum, $I\left(k_x\right)$, is accumulated at $k_x = 0$. Further, the temporal spectrum $I(\omega)$ shows indications that it becomes discrete. This last effect can also be observed reversing the coupling to higher order modes, in (g) and (h), where the spectrum in k_x clearly exhibits an energy transfer to higher modes. For an outwards coupling, the field in direct space, (g), follows the modulation, but being quantitatively less regular than for a symmetric Hermitian modulation, seen (c). For all the cases, the red arrows in the spectra correspond to the couplings introduced by the potential. While the solid ones represent functional couplings, the dashed ones correspond to non-functional ones, since they couple resonant modes to non-resonant ones (modes far from the dispersion curve).

In order to determine the dependency of the effect on the phase shift, we map the three different parameters η, $FWHM_{k_x}$ and $FWHM_\omega$ in the $\left(m, \phi_t\right)$ space in Fig. 4 (a)–(c). The same tendency is qualitatively observed for the three magnitudes, although the condensation to the homogeneous state, (a) has a clearer trend. In (d) and (e) we show the spectra $I\left(k_x\right)$ and $I(\omega)$ for different parameter sets labelled as (i) and (ii) in the maps as well as the unmodulated spectrum in black. Two different dynamical regimes of the system can be clearly distinguished,

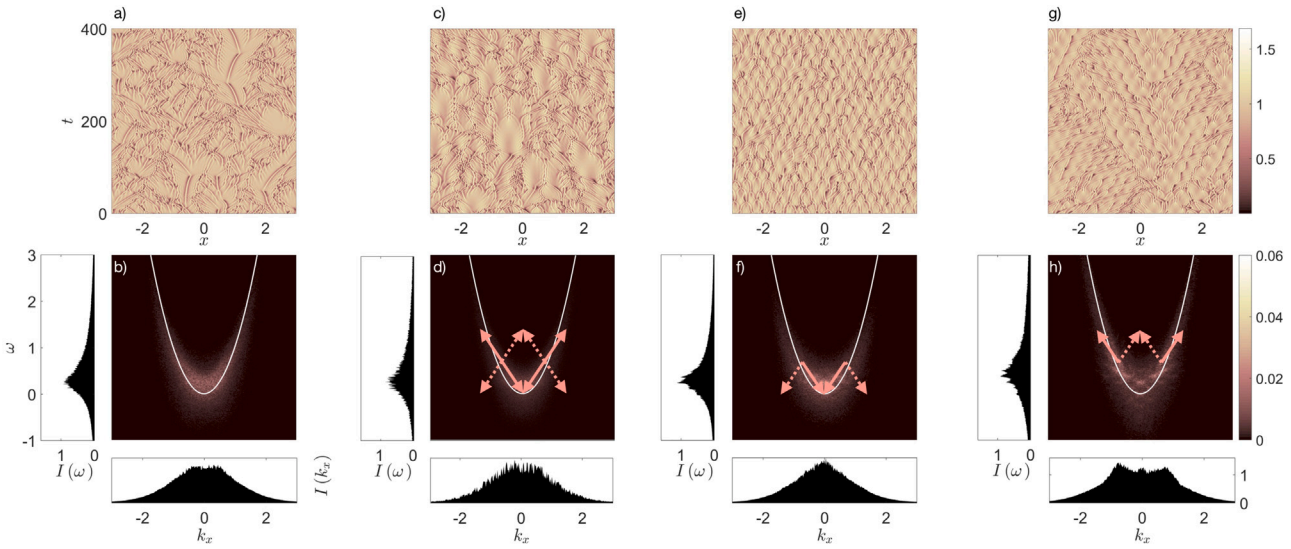

Fig. 3. Turbulence control for parabolic dispersion. Temporal evolution of the field intensity and corresponding spatio-temporal Fourier power spectrum $\left|A\left(k_x,\omega\right)\right|^2$ for (a)/(b) no modulation, (c)/(d) symmetric modulation, and modulations with (e)/(f) inward and (g)/(h) outward functional couplings. The curve represents the parabolic dispersion $\omega = k_x^2$. Insets correspond to integrals of the spectrum intensity over ω and k_x, respectively. Red arrows in (d)/(f) and (h) indicate all possible functional (in solid) and non-functional (in dashed) mode couplings associated to the corresponding potential. Eq. (1) is integrated for $\alpha = 0.7$, and $d = 0.03$. The parameters of the potential in (c)–(h) are: $\omega = 0.12$, $q = 0.356$, and $m = 0.2$.

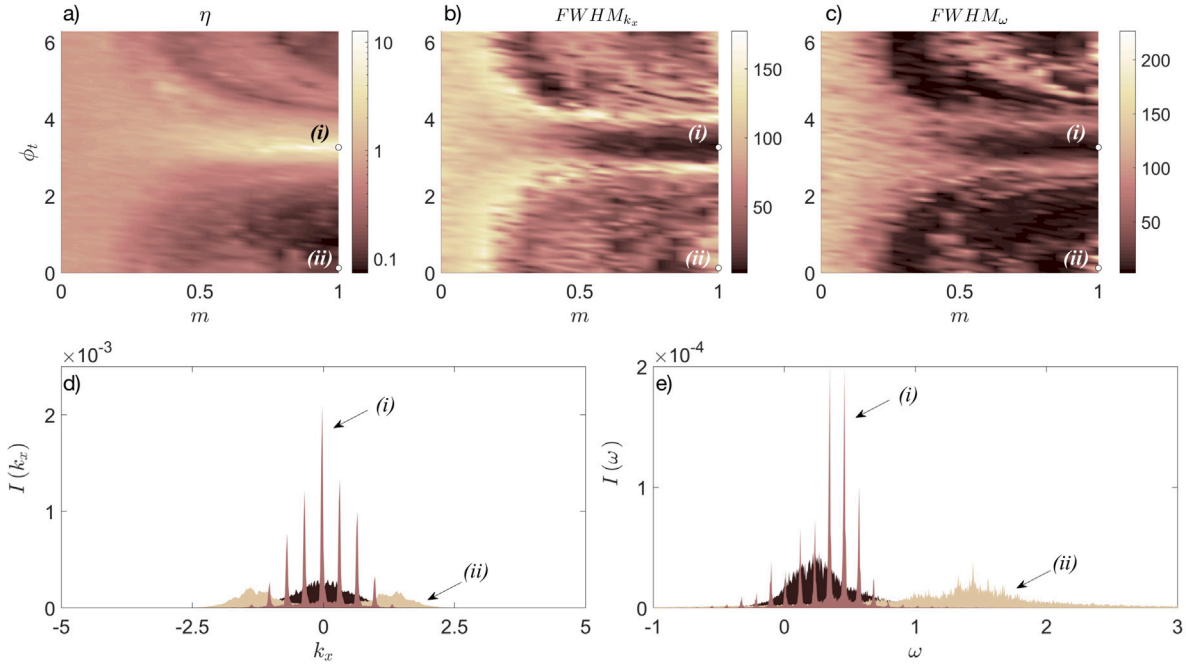

Fig. 4. Parameter analysis for parabolic dispersion. Maps in (m_2, ϕ_t) parameter space of: (a) the normalised central intensity, (b) FWHM of the sorted averaged spectrum in k_x, and (c) in ω, respectively. Averaged spectrum intensity in: (d) ω, and (e) k_x, respectively. Labels (i) and (ii) indicate points in (a)–(c) maps represented in plots (d) and (e). Black spectrum corresponds to the unmodulated turbulent field. We assume: $\alpha = 0.7$ $d = 0.03$, $\omega = 0.12$, $q = 0.356$ for all plots.

first, for (i) with a phase shift around $\phi_t = \pi$ and corresponding to a coupling towards lower order modes, we see a clear $I\left(k_x\right)$ condensation at $k_x = 0$. Differently, the coupling to higher order modes corresponds to phase shifts with values around $\phi_t = 0$ and clearly produce a broadening of the spectrum. In the temporal domain, the spectrum is also regularised coinciding with a spatial turbulence reduction. On the contrary, when turbulence is increased, the spectrum shifts to higher values of ω with a higher dispersion of frequency values, as expected. In these particular calculations we have fixed the value of $q = 0.335$ and $\Omega = q^2$, although as shown in [18] the range of working (q, Ω) is quite large.

3.2. Conical dispersion $\beta = 1$

Next, we reproduce the study done for a parabolic dispersion for media with conical dispersion $\beta = 1$. In Fig. 5 (a) and (b) we provide the field and its spectrum for an unmodulated system. The turbulent spectrum corresponds to a distribution of points in $\left(k_x, \omega\right)$ that follows the dispersion lines $\omega = \left|k_x\right|$ for large k_x values. However, in this case the turbulent spectrum is not maximum at $k_x = 0$ but we can observe two lobes. This hints that the condensation of the energy at the homogeneous state will not be the best parameter to characterise the effect of the modulation we are introducing. Again, the introduction

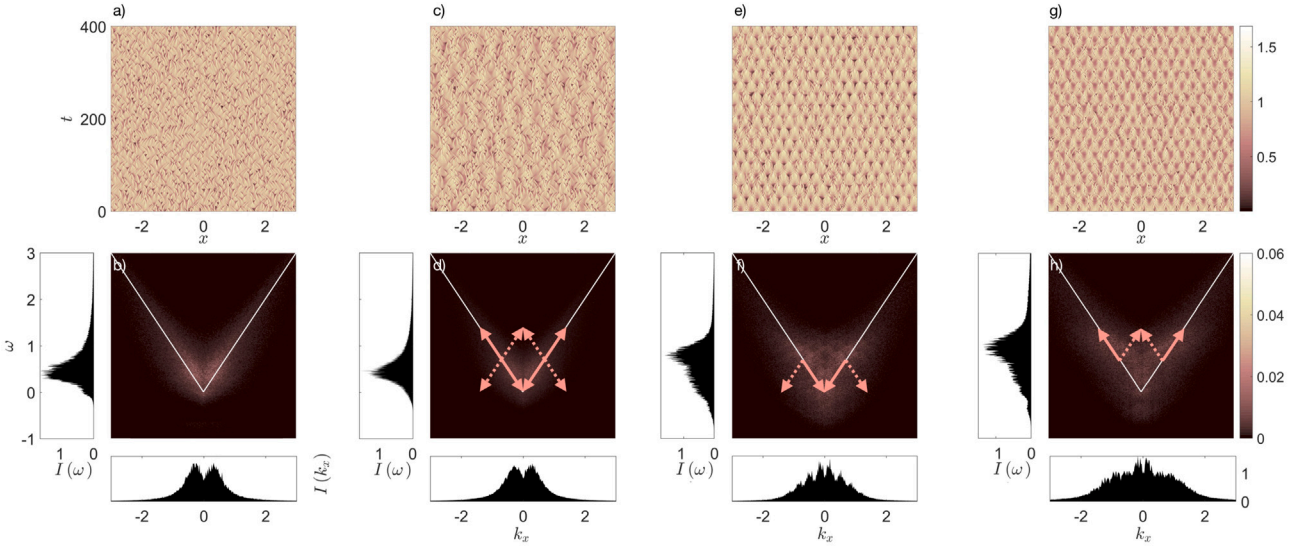

Fig. 5. Turbulence control for conical dispersion. Temporal evolution of the Field intensity and corresponding Intensity of the spatio-temporal Fourier spectrum $\left|A\left(k_x,\omega\right)\right|^2$ for: (a)/(b) no modulation, (c)/(d) a symmetric modulation, and (e)/(f) modulations with inward and (g)/(h) outward functional couplings. The white straight lines represent the conical dispersion $\omega = |k_x|$. Insets correspond to integrals of the spectrum intensity over ω and k_x, respectively. Red arrows in (d), (f) and (h) indicate all possible functional (in solid) and non-functional (in dashed) mode couplings associated to the corresponding potential. $q = 0.356$, $\omega = 0.12$, $\alpha = 0.7$ and $d = 0.03$ for all plots. $m = 0.2$ for (c)–(h).

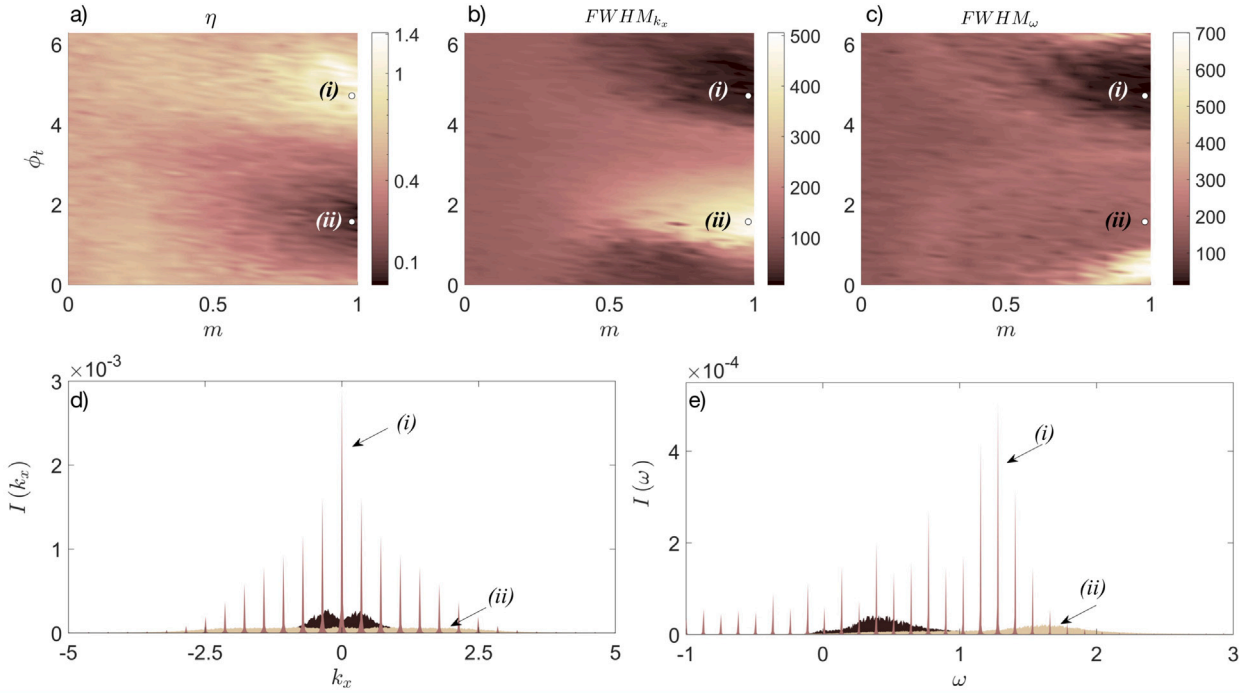

Fig. 6. Parameter analysis for conical dispersion. Maps in $\left(m_2,\phi_t\right)$ parameter space of: (a) the normalised central intensity, (b) FWHM of the sorted averaged spectrum in k_x, and (c) in ω, respectively. Averaged spectrum intensity in: (d) ω, and (e) k_x, respectively. Labels (i) and (ii) indicate points in (a)–(c) maps represented in plots (d) and (e). Black spectrum corresponds to the unmodulated turbulent field. We assume: $\alpha = 0.7$ $d = 0.03$, $\omega = 0.12$, $q = 0.356$ for all plots.

of a potential with a Hermitian modulation introduces such modulation in the field evolution, shown in (c) but, since the coupling is symmetric in space and time, the distribution of excited modes in Fourier spectra is approximately the same as the one of the unmodulated case. For the non-Hermitian modulations, we check that functional coupling to the lower modes, (e) and (f), tends to concentrate the spectrum at around $k_x = 0$ while functional couplings to higher modes tends to make the spectrum more broaden, (g) and (h).

To do a systematic study we also map the three values, η, $FWHM_{k_x}$ and $FWHM_{\omega}$ in the $\left(m,\phi_t\right)$ space in Fig. 6 (a)–(c). We clearly see the same tendency for the three magnitudes although $FWHM$ presents a stronger dependency on phase shift than the parabolic case. This difference is due to the sharper harmonics generated by the non-Hermitian modulation in conical dispersion. Looking at the spectra of the two examples (i) and (ii) indicated in (a)–(c), we clearly see for (i), the strong energy accumulation at harmonics of the potential frequency and it corresponds to a small $FWHM$ values, while for (ii) we see a strong broadening of the spectrum. In comparison with the parabolic case, the effect of the potential in the conical case is dramatically increased. It is easily detected by looking to the spatial and temporal spectra and this difference is directly translated to an increase of the $FWHM$ contrast. Further, the difference is visible in

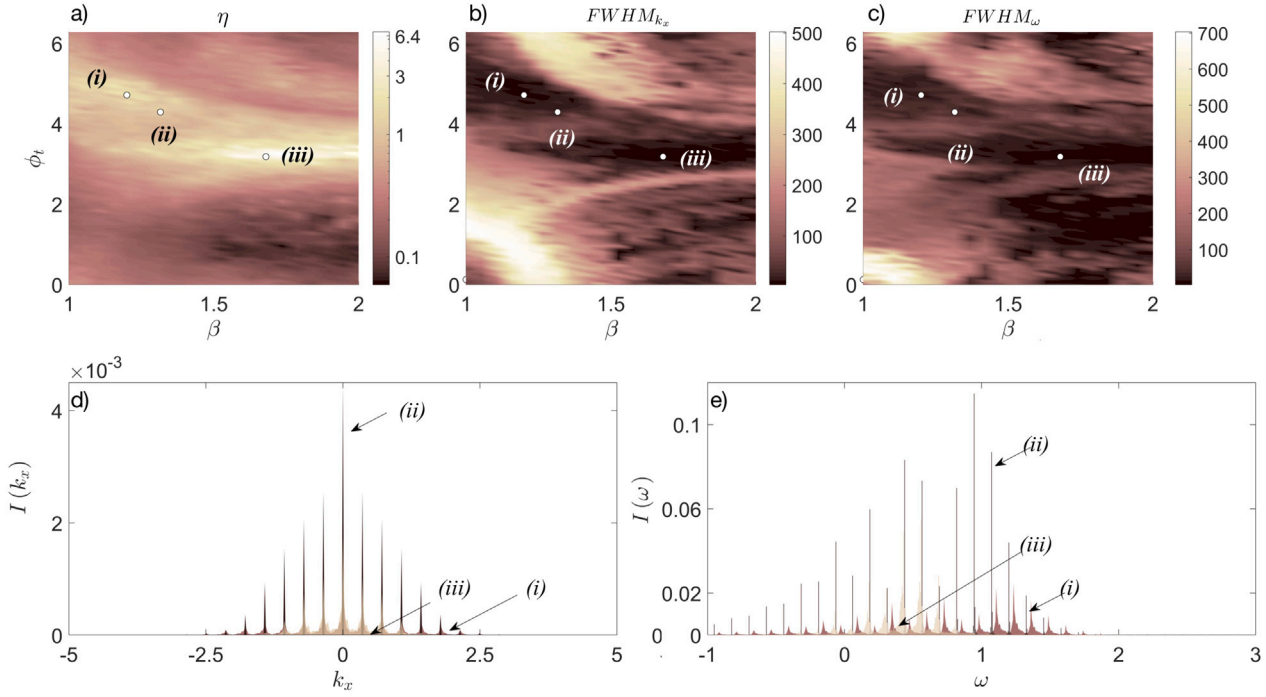

Fig. 7. Control of the turbulent spectrum for fractional dispersion. (a)–(c) (β, ϕ_t) maps of the normalised central intensity, FWHM of the sorted averaged spectrum in k_x and in ω respectively. (d) and (e) averaged spectrum intensity in ω and k_x respectively for parameters corresponding to points (i)–(iii) in the (a)–(c) maps. $q = 0.356$, $\omega = 0.12$, $m = 1$, $\alpha = 0.7$ and $d = 0.03$ for all plots.

the ratio of the field concentrated at $k_x = 0$ but also on the number of relevant coherently excited harmonics. This may be due to the fact that now, the dispersion relation is composed by straight lines and a given coupling arrow acts equally for all k_x. Another important difference from the parabolic dispersion is the phase shift corresponding to the largest turbulence reduction, happening in the conical case around $\phi_t = 3\pi/2$ and around $\phi_t = \pi$ for the parabolic one. Equivalently, the phase difference repeats for the maximum broadening, around $\phi_t = \pi/2$ for the canonical case.

3.3. Non-integer fractional dispersion $\beta \notin \mathbb{N}$

The turbulence control by non-Hermitian spatio-temporal potentials acts in the system by introducing directional couplings in the wavenumber–frequency space. This general mechanism can be applied to any dispersion relation and in particular to fractional dispersions. Aside, as observed in previous sections, the optimal ϕ_t value to reduce turbulence is different for parabolic and conical dispersions, around $\phi_t = \pi$ and around $\phi_t = 3\pi/2$ respectively. We explore the turbulence control in fractional dispersions by scanning the fractional power β and the temporal phase shift of the modulation ϕ_t and mapping η, $FWHM_{k_x}$ and $FWHM_\omega$ in the (β, ϕ_t) space for a fixed value of $m = 1$ and fixed values of $q = 0.335$ and $\Omega = 0.12$, as it is shown in Fig. 7 (a)–(c). We observe that far to be a step function, the optimal ϕ_t value suffers a soft decrease when β is scanned from 1 to 2. The stabilisation effect is present for any fractional dispersion as shown by the spatial and temporal spectra in (d) and (e). They correspond to different points $(i)-(iii)$ of the parameter space along the optimal curve. The effect is the same, a regularisation in both space and time spectra and an accumulation of $I(k_x)$ at $k_x = 0$. We note that further increasing β the phase shift tends asymptotically to π.

3.4. Fourth order dispersion $\beta = 4$

We finally test the robustness of proposed mechanism for sub-diffractive cases, in particular for fourth order dispersion $\beta = 4$. We note that the stabilisation is improved for values of q that differ from the previous studied situations. Therefore, we study the dependency of the effect of the modulation in the (q, ϕ_t) parameters space. We here use only the condensation at the homogeneous solution, η, since we have seen that for values of β greater than 1.5 this parameter is the best one due to the distribution of the unmodulated spectrum. The map in Fig. 8 (a) indeed shows that the range of optimal values is shifted towards lower values of the spacial frequency modulation. This may be attributed to the fact that the spectrum of the turbulence is more concentrated at lower values of ω due to the shape of the dispersion. We have chosen five points in the map, *i.e.* five pairs of parameters, $(i)-(v)$ to illustrate the effect of the potential on the resulting spectra. Figs. 8 (b) and (c) provides the spatial and the temporal spectrum respectively, $I(k_x)$ and $I(\omega)$. We note that for parameters in the whitish area, $(i)-(iii)$, the effect of the potential regularises the spectrum, both in space and time see the inset in Fig. 8 (c). In turn, for bad concentrations of energy at $k_x = 0$, (iv) and (v), we have observed two different behaviours. While there is always a clear spectral broadening in space and time, only for (v) a discretisation in time occurs.

3.5. Higher dimensional system

After focusing on the study of the 1D system, we here provide examples of the extension to 2D. Naturally, introducing more dimensions the computational time increases, and this is the reason behind the previous exhaustive study being restricted to 1D. The proposal and some of the results can be straightforwardly generalised to higher-dimensional systems. For instance, in Fig. 9 we provide a highlight of results in 2D system with parabolic dispersion, see Fig. 9 (a) and (b), along with 2D results for conical dispersion, in Fig. 9 (c) and (d). We introduce the spatial part of the potential in the form: $V(\mathbf{r}) = 1/n \sum_{i=1}^{n} \cos(\mathbf{q_i r})$, where $\mathbf{q_i}$ correspond to the lattice vectors. We here focus on the simplest 2D modulation with square geometry, i.e. $\mathbf{q_1} = q[1, 0]$ and $\mathbf{q_2} = q[0, 1]$. In Fig. 9 (a) and (d) we see the averaged 2D Fourier Transform of the field for the unmodulated case. When introducing the modulation, for $m = 1$, we clearly observe that the

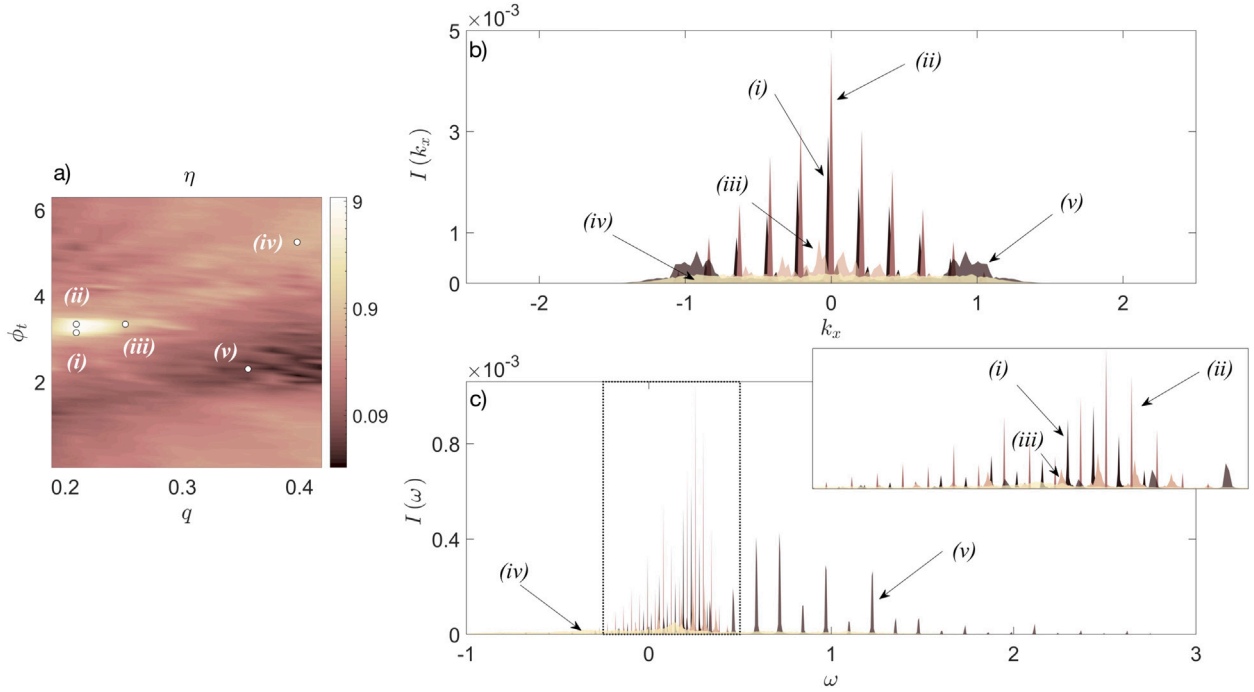

Fig. 8. Control of the turbulent spectrum for fourth order dispersion. (a) (q, ϕ_t) maps of the normalised central intensity. (b) and (c) averaged spectrum intensity in k_x and ω respectively. Labels (i)–(v) in the different spectra correspond to parameter pairs in (a). The inset corresponds to the area marked in the rectangle. $\omega = q^2$, $m = 1$, $\alpha = 0.7$ and $d = 0.03$ for all plots.

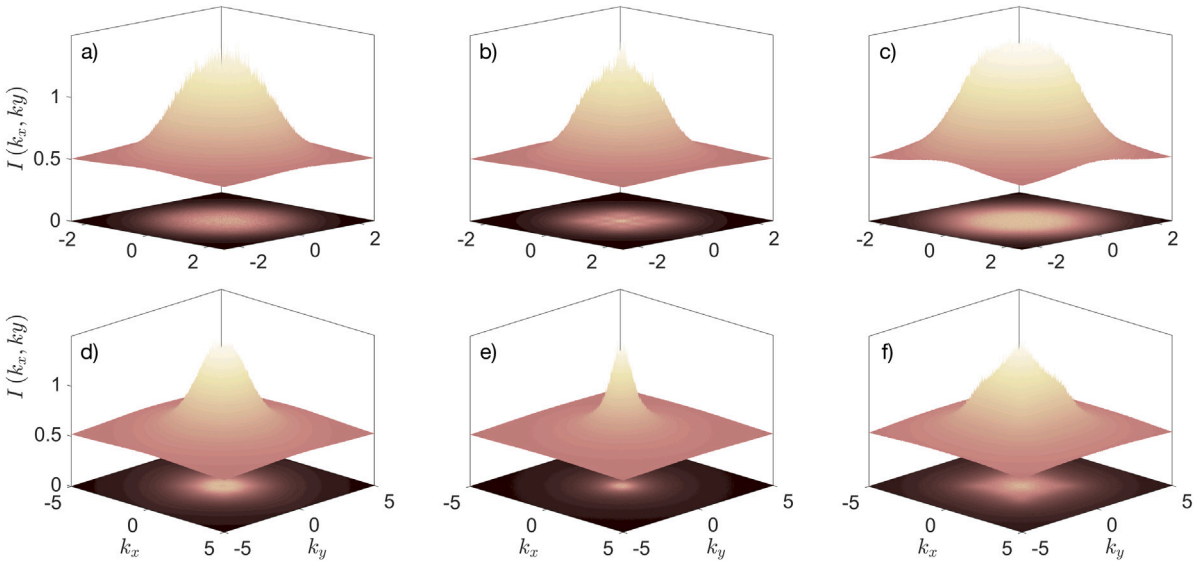

Fig. 9. 2D Turbulence spectra. Top row corresponds to system with $\beta = 2$ and bottom row to $\beta = 1$. First column shows the spectrum for the unmodulated system, while second and third columns correspond to the modulated case for inward and outward coupling. Parameters are the same as the ones in Fig. 6.

narrowing of the spectrum, which condensates the energy towards the low order mode. This occurs for a complex phase delay $\phi_t = \pi$ for a parabolic dispersion and for $\phi_t = 3\pi/2$ for the conical dispersion see Fig. 9 (b) and (e). Moreover, we can also observe the broadening of the spectrum for $\phi_t = 0$ and $\phi_t = \pi/2$ for the different types of diffraction respectively. This scenario is depicted in Fig. 9 (c) and (f). Qualitatively, the effect is perfectly analogous the one demonstrated in 1D. Moreover, we observe how the effect on the conical case is notably enhanced, just as for 1D. Particularly, for parabolic dispersion, a wider study for different spatial configurations with more lattice vectors can be found in [18].

4. Conclusions

To conclude, we have proposed a mechanism to influence the energy cascade that governs turbulence leading to a reduction of the turbulent spatio-temporal spectra. Indeed, the introduction a periodic spatio-temporal potential, being non-Hermitian in time, may induce an asymmetric mode coupling towards lower frequencies and smaller wave numbers, reducing the cascade of turbulence, and eventually regularising the spectra. In turn, it is also possible to induce an inverse cascade which broadens the spectrum, enhancing turbulence. In this last situation, the potential favours coupling towards higher frequencies and larger wave numbers enhancing the cascade and thus broadening

the spectrum. We provide a comprehensive analysis of the control mechanism on the universal CGLE which governs optical turbulence, among other physical systems, and we extend it to the FCGLE. The idea is proven on 1D systems with different dispersion: parabolic (quadratic), conical (linear), but also for general dispersion involving non-integer partial derivatives and for sub-diffracting dispersion, for instance fourth-order. For all cases, the turbulence control mechanism is robust for a wide range of parameters being mainly governed by the phase shift between the real and imaginary parts of the complex temporal potential, and their modulation amplitude. We note that we assumed a fixed value for the spatial periodicity (and frequency) which is not necessarily the optimal one, and scanned the required phase and modulation amplitude for the effect to happen. We observe that while for the parabolic case the spatio-temporal spectrum is condensed for $\phi_t = \pi$, for conical dispersion a significant regularisation of the spectrum – both in space and time – is found for a value of the complex phase shift of $\phi_t = 3\pi/2$. The analysis of the general fractional CGLE provides a good agreement with these previous results, when scanning such phase as a function of the differential power. Finally, we observe that for the sub-diffracting case, the periodicity required to regularise the field is smaller than in the previous ones, yet the mechanism provides the concentration of energy at lower modes, and even when the spectrum broadens a discretisation of the temporal frequencies occurs. In principle, for being proved on the FCGLE, as the generalisation of a universal mathematical model in physics, the present turbulence control scheme may have applications in different physical systems.

CRediT authorship contribution statement

Salim B. Ivars: Software, Data curation, Writing – review & editing. **Muriel Botey:** Writing – review & editing. **Ramon Herrero:** conceptualization, Writing – review & editing. **Kestutis Staliunas:** conceptualization, Writing – review & editing.

Declaration of competing interest

The authors declare that they have no known competing financial interests or personal relationships that could have appeared to influence the work reported in this paper.

Data availability

No data was used for the research described in the article.

Acknowledgements

This work received funding from the Spanish Ministerio de Ciencia e Innovación under Grant No. 385 (PID2019-109175GB-C21). from European Social Fund (Project No. 09.3.3- LMT-K712-17- 0016) under a grant agreement with the Research Council of Lithuania (LMTLT), and from the European Union's Horizon 2020 Research and Innovation Programme under the Marie Skłodowska-Curie grant agreement No 861152.

References

[1] Landau LD. Dokl Akad Nauk USSR 1944;44:311.
[2] Kolmogorov AN. Cr Acad Sci URSS 1941;30:301–5.
[3] Richardson LF. Weather prediction by numerical process. Cambridge University Press; 2007.
[4] Sommerfeld A. Ein beitrag zur hydrodynamischen erklaerung der turbulenten fluessigkeitsbewegungen. 1909.
[5] Lorenz EN. J Atmos Sci 1963;20(2):130–41.
[6] Kolmogorov AN. Proc Royal Soc Lond Ser A 1991;434(1890):15–7.
[7] Staliunas K, Sanchez-Morcillo VJ. Transverse patterns in nonlinear optical resonators, vol. 183. Springer Science & Business Media; 2003.
[8] Tlidi M, Staliunas K, Panajotov K, Vladimirov A, Clerc M. Phil Trans R Soc A 2014;372(2027):20140101.
[9] Tlidi M, Clerc MG. Springer Proc Phys 2016;173.
[10] Brambilla M, Cattaneo M, Lugiato L, Pirovano R, Prati F, Kent A, et al. Phys Rev A 1994;49(2):1427.
[11] Brambilla M, Battipede F, Lugiato L, Penna V, Prati F, Tamm C, et al. Phys Rev A 1991;43(9):5090.
[12] Battogtokh D, Mikhailov A. Physica D 1996;90(1–2):84–95.
[13] Casal AC, Díaz JI. Recent trends in chaotic, nonlinear and complex dynamics. World Scientific; 2022, p. 455–513.
[14] Tafo JBG, Nana L, Tabi CB, Kofané TC. Research advances in chaos theory. IntechOpen; 2020.
[15] Xiao J, Hu G, Yang J, Gao J. Phys Rev Lett 1998;81(25):5552.
[16] Zhang H, Hu B, Hu G, Ouyang Q, Kurths J. Phys Rev E 2002;66(4):046303.
[17] Jiang M, Wang X, Ouyang Q, Zhang H. Phys Rev E 2004;69(5):056202.
[18] Ivars SB, Botey M, Herrero R, Staliunas K. Phys Rev A 2022;105(3):033510.
[19] Aranson IS, Kramer L. Rev Modern Phys 2002;74(1):99.
[20] Bartuccelli M, Constantin P, Doering CR, Gibbon JD, Gisselfält M. Physica D 1990;44(3):421–44.
[21] Montagne R, Hernández-García E, Amengual A, San Miguel M. Phys Rev E 1997;56(1):151.
[22] Iwasaki H, Toh S. Progr Theoret Phys 1992;87(5):1127–37.
[23] Picozzi A, Garnier J, Hansson T, Suret P, Randoux S, Millot G, et al. Phys Rep 2014;542(1):1–132.
[24] Ahmed W, Herrero R, Botey M, Staliunas K. Phys Rev A 2016;94(5):053819.
[25] Ahmed W, Herrero R, Botey M, Hayran Z, Kurt H, Staliunas K. Phys Rev A 2018;97(3):033824.
[26] Bender CM, Boettcher S. Phys Rev Lett 1998;80(24):5243.
[27] Staliunas K, Peckus M, Sirutkaitis V. Phys Rev A 2007;76(5):051803.
[28] Peckus M, Rogalskis R, Andrulevicius M, Tamulevicius T, Guobiene A, Jarutis V, et al. Phys Rev A 2009;79(3):033806.
[29] Staliunas K, Herrero R, Vilaseca R. Phys Rev A 2009;80(1):013821.
[30] Staliunas K, Herrero R, de Valcárcel GJ. Physica D 2009;238(15):1326–37.
[31] Hatsugai Y, Fukui T, Aoki H. Eur Phys J Spec Top 2007;148(1):133–41.
[32] Laskin N. Phys Lett A 2000;268(4–6):298–305.
[33] Weitzner H, Zaslavsky G. Commun Nonlinear Sci Numer Simul 2003;8(3–4):273–81.
[34] Herrmann R. Fractional calculus: An introduction for physicists. World Scientific; 2011.
[35] Guo X, Xu M. J Math Phys 2006;47(8):082104.
[36] Qiu Y, Malomed BA, Mihalache D, Zhu X, Zhang L, He Y. Chaos Solitons Fractals 2020;131:109471.
[37] Tarasov VE, Zaslavsky GM. Physica A 2005;354:249–61.